IEEE Access
Multidisciplinary | Rapid Review | Open Access Journal

Received 30 December 2023, accepted 9 January 2024, date of publication 15 January 2024, date of current version 24 January 2024.

Digital Object Identifier 10.1109/ACCESS.2024.3354169

METHODS

Underwater Image Enhancement via Adaptive Color Correction and Stationary Wavelet Detail Enhancement

ZHENBO WANG, DUJUAN ZHOU, ZHICHUANG LI, ZIZHAO YUAN, AND CHUN YANG
Beijing Institute of Technology, Zhuhai 519088, China

Corresponding author: Dujuan Zhou (17424@bitzh.edu.cn)

This work was supported in part by the Key Platform and Scientific Research Project for General Universities, Guangdong, in 2022, under Grant 2022ZDZX4061; in part by the University Students Science and Technology Innovation Cultivation Special Fund Project, Guangdong, in 2023, under Grant pdjh2023a0610; in part by the Science and Technology Program of Social Development, Zhuhai, in 2022, under Grant 2220004000195; in part by the Key Area Special Project for Ordinary High Schools (New Generation Information Technology), Guangdong, under Grant 2023ZDZX1045; in part by the Department of Education Special Innovative Project, Guangdong, under Grant 2022KTSCX197; in part by the Philosophy and Social Sciences Planning Project, Zhuhai, in 2023, under Grant 2023GJ087; in part by the Innovation and Entrepreneurship Training Programme for University Students Project, China, in 2023, under Grant 2023001DCXM.

ABSTRACT High-quality images are of great significance for vision tasks in underwater environments. However, as light propagates through water, it is scattered and absorbed, which commonly causes issues like color distortion and loss of detail, making the capture of high-quality images challenging. To improve the quality of underwater images, we propose an underwater image enhancement method that is based on channel similarity to adaptive color correction and stationary wavelet detail enhancement. Specifically, We first innovatively introduce channel similarity values to avoid red artifacts during color correction, and finely adjust the compensation amount at the pixel level based on the intensity difference between the red and green channels. By designing a new dynamic normalization range based on channel similarity, our color correction method adaptively adjusts the dynamic range of each RGB channel's pixel value. This accommodation for color deviations in various underwater scenes enhances the color saturation of images. Subsequently, using the stationary wavelet transform, we accurately decompose the image into low-frequency and high-frequency components. Through fine processing of the low-frequency components, we optimize detail performance and enhance the visual clarity of the underwater scene. Extensive experiments on four benchmark datasets validate that our method is state-of-the-art in underwater image enhancement, excelling in both qualitative and quantitative evaluations. Additionally, our method bolsters the precision of tasks such as keypoint matching and edge detection within the realm of image processing. The code is available at https://github.com/Zhenbo-Wang/Adaptive-Color-Correction-and-Stationary-Wavelet-Detail-Enhancement.

INDEX TERMS Underwater image enhancement, color correction, channel similarity, stationary wavelet decomposition.

I. INTRODUCTION

The oceans, rivers, and lakes are repositories of extensive biodiversity and natural resources. Recent advancements in science and technology have established image processing and analysis as crucial tools, expanding the capabilities of researchers to explore and study underwater environments. These methodologies are extensively utilized in areas such as marine biology research [1], surveys of underwater environments and resources [2], the inspection and maintenance of

The associate editor coordinating the review of this manuscript and approving it for publication was Felix Albu.

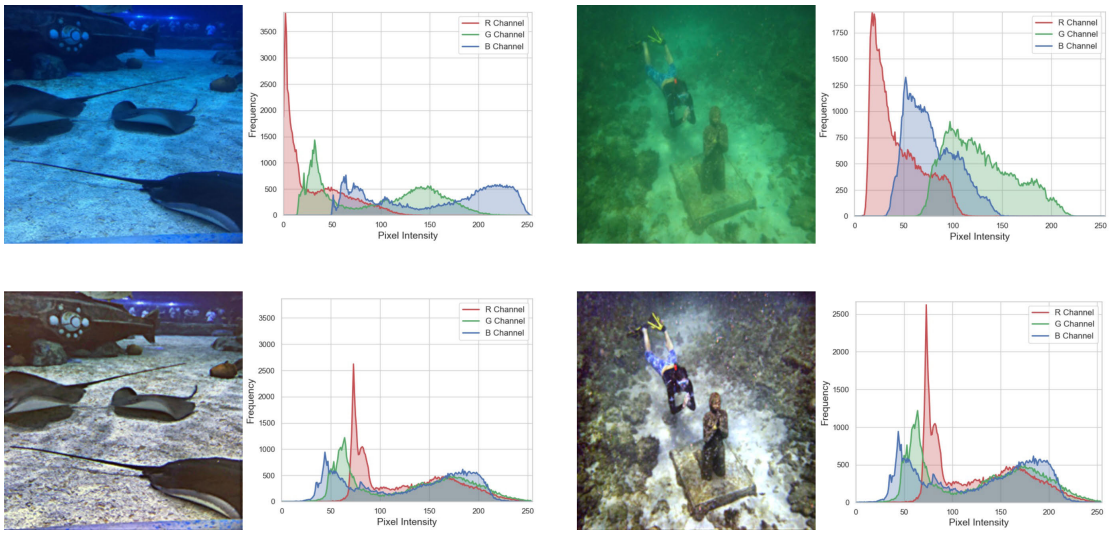

FIGURE 1. Comparison of original and enhanced images and their color distribution histograms. The first row shows the original images and their color distribution histograms, and the second row shows the enhanced images and color distribution histograms by our method.

subaquatic structures [3], underwater archaeological exploration [4], and the development of underwater robotics [5]. However, the complexity of the underwater environment makes it difficult for ordinary imaging equipment to capture clear underwater images.

The quality of underwater images is influenced by a number of factors, primarily the inherent attributes of the aquatic environment and the physical processes governing light propagation within this medium. These factors can lead to problems such as color distortion, low contrast, loss of detail, blurred images. For instance, light of different wavelengths exhibits varied attenuation rates when propagating underwater. Due to the longer wavelength of red light, it is easily absorbed by water, while blue-green light, with its shorter wavelengths, has a stronger propagation capability. Therefore, underwater, the intensity of red light diminishes swiftly, whereas the blue and green light maintains a stronger intensity relative to red [6]. As shown in the first row of color distribution histograms in Figure 1, the average pixel value of the red channel is smaller than the average pixel value of the blue and green channels, which makes most of the underwater images we obtain show a greenish hue or a bluish hue. Light propagating underwater also undergoes scattering, which causes the light to deviate from its original straight-line path, resulting in blurred images. In addition, suspended particles and organisms in the water further enhance scattering and absorption, resulting in reduced image contrast and loss of detailed information [7]. Thus, the research on obtaining high-quality underwater images by means of underwater image enhancement methods has become an urgent problem for underwater vision, which is of great significance for enhancing the efficiency and accuracy of underwater activities, protecting marine life and cultural heritage, and promoting scientific research and industrial development.

In this work, we propose an enhancement method based on channel similarity to adaptive color correction and stationary wavelet transform to address the problem of color distortion, contrast degradation, and detail loss in underwater images. The main contributions of this paper are as follows.

- We propose a method based on channel similarity and red channel compensation, which introduces the channel similarity value to determine whether the red channel needs to be compensated or not, and effectively avoids red artifacts in color correction. In addition, the amount of compensation is finely adjusted at the pixel level based on the intensity difference between the red and green channels. This method provides an innovative and targeted solution to the problem of image color distortion in underwater environments.
- We design a new normalization range for statistical color correction based on channel similarity, which makes our correction method can be adaptively adjusted according to the unique color distribution of each image, thus further enhancing the contrast and saturation of the image.
- We present a combined strategy of stationary wavelet decomposition and image sharpening. The approximate low-frequency components of the image are extracted by the translation invariance of the stationary wavelet, and then sharpening the low-frequency information can effectively enhance the main structure and morphology of the image, improving the local details of the image.

II. RELATED WORK

Currently, underwater image enhancement technology can be divided into two research directions: hardware enhancement and algorithm enhancement. Hardware enhancement mainly relies on advanced optical and electronic devices to improve

the quality of image acquisition, such as sonar technology [9] and polarization technology [10]. Sonar techniques are capable of accurately determining the distance between an underwater object and the camera and correcting for perspective distortion caused by the refraction of light in water. Polarization techniques are applied to complex scattering situations in water to effectively reduce or eliminate the effects of scattering caused by various suspended particles. While hardware enhancement methods perform well in certain specific contexts, they are often accompanied by expensive equipment costs, complex maintenance requirements and portability. In addition, hardware methods may not be able to meet the challenges of all underwater environments and conditions.

Compared with hardware enhancement, algorithmic enhancement not only solves the problems of cost and complexity, but also provides more flexible and diversified means of image processing, making it more advantageous and attractive in many application scenarios. Algorithmic enhancement methods are mainly classified into three underwater image enhancement techniques based on physical models, non-physical models, and deep learning [11].

(1) Physical model-based underwater image enhancement techniques aim to develop mathematical models to describe the physical process of underwater image degradation as a basis for designing algorithms for image processing and enhancement. For example, the Jaffe-McGlamery underwater imaging model [12] describes in detail the image quality degradation process due to light scattering and absorption in underwater optical imaging, which is a classical model in underwater vision research. Chiang et al. compensated for the attenuation differences in the propagation path, thus improving the quality and sharpness of underwater images [13], [14]. In addition, Drews et al. utilized the theoretical basis of the physical light propagation model [15] to improve the quality of underwater images by designing a depth estimation method to create a depth map for underwater images, then estimating and removing the background scattering based on the depth value of each pixel, and finally automatically adjusting the global color distribution of the image through a color correction method. Akkaynak and Treibitz proposed a method called Sea-Thru [16], which demonstrates through physical modeling that the attenuation coefficient of the signal is not uniformly distributed throughout the scene, but depends on the distance and reflectivity of the object. They further showed that the coefficient of backscattering increasing with distance is different from the signal attenuation coefficient. This approach successfully solves the problem of color loss caused by commonly used atmospheric image formation models when applied to underwater images.

(2) Non-physical modeling techniques for underwater image enhancement are used to improve image quality by directly adjusting image pixel values. Typical representative methods include histogram equalization [23], contrast stretching [17], image fusion [19], [41] and Retinex-based methods [21], [22], [28]. For example, Iqbal, Kashif et al. proposed a color balance and contrast correction method based on RGB and HSI color models [17], aiming to reduce color bias and improve image quality. To address the problem of color bias in underwater images, Dong et al. proposed a specific fraction-based method [18] that combines the application of RGB and LAB color models to optimize the image quality by performing color correction in both RGB and LAB color spaces, while enhancing the contrast in the L-channels and applying a strategic equalization in the AB-channels. Ancuti et al. proposed a method combining the underwater white balance technique and multi-scale fusion technique [19], which can effectively improve the quality of underwater images. Recently, Zhang et al. proposed an underwater image enhancement method called MLLE [20], which locally adjusts the color and details of the input image according to the principle of minimum color loss and the fusion strategy guided by the maximum decay map, and adaptively adjusts the contrast of the image through the local mean and variance to further improve the visibility of the image.

(3) With the rapid development of deep learning technology in recent years, underwater image enhancement techniques based on deep learning have also been widely applied [24], [25], [26]. To address the problem of monocular underwater image color correction, Li et al. proposed a generative adversarial network called WaterGAN [24]. This network achieves color correction of monocular underwater images by generating a training dataset using real underwater images and their corresponding depth information, and further using these data to train WaterGAN. Similarly, Jiang et al. proposed a goal-directed perceptual adversarial fusion network named TOPAL based on adversarial networks and image fusion [25], which achieves adaptive fusion of latent features through dual-channel attention modules and introduces a global-local adversarial mechanism in the reconstruction, thus significantly improving the quality of underwater images. Peng et al. designed a U- shape transformer network [26], which integrates channel-wise and spatial-wise attention mechanism modules to effectively eliminate color artifacts and colors. Huang et al. proposed a semi-supervised learning framework called Semi-UIR [27], which consists of a teacher network and a student network. This framework aims to exploit the extra information contained in unlabeled data to improve the performance and generalization of the model. Although deep learning-based image enhancement methods exhibit significant potential and advantages, they also face some challenges. The existing deep learning-based underwater image enhancement methods are limited by the lack of a large amount of real training data and a priori information, as well as the possibility of ignoring underwater-specific problems, which together limit the efficacy and usability of deep learning-based underwater image enhancement methods,

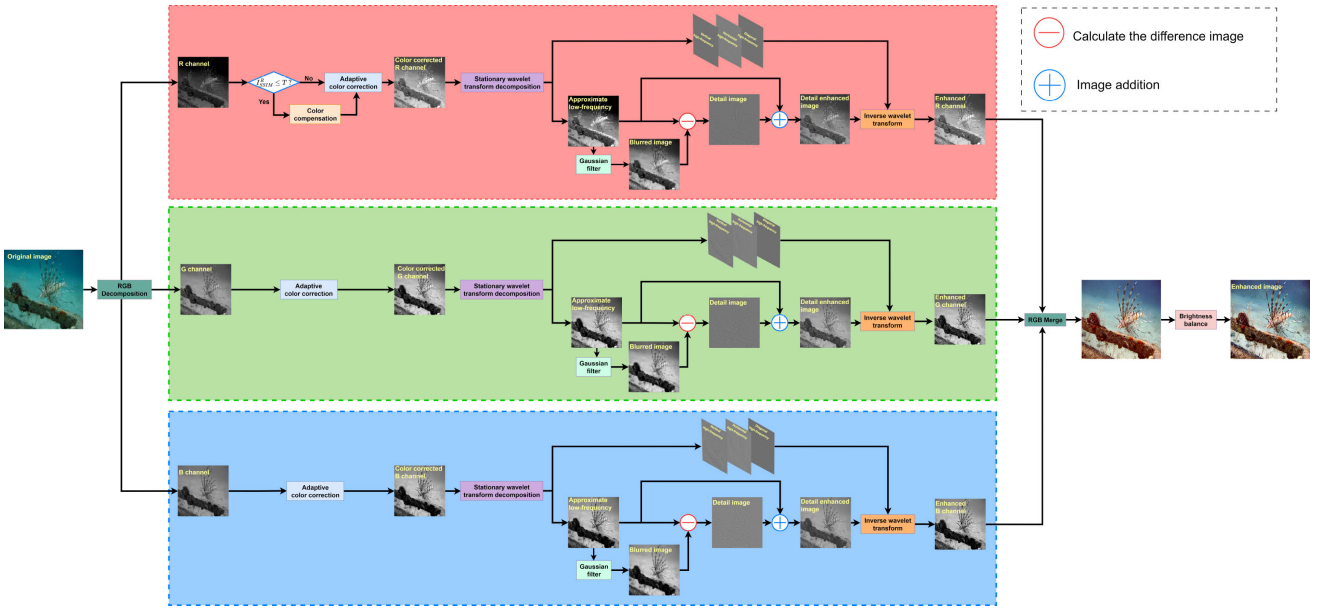

FIGURE 2. Flowchart of the proposed method.

FIGURE 3. Visualization of color channel separation. The red channel loses a lot of information, while the green and blue channels retain more image information.

resulting in less robustness and generalization than traditional methods.

III. METHOD

We present the flowchart of our method in Figure 2. The proposed method includes three main steps: red channel color compensation, color correction of RGB channels and stationary wavelet transform enhance details. In this section, our method is described in detail.

A. RED CHANNEL EVALUATION AND COMPENSATION

The longer wavelengths of red light are easily scattered and absorbed in water, resulting in rapid attenuation and severe loss of visual information. In contrast, the shorter wavelengths of blue and green light attenuate more slowly in water, so their information is better retained underwater, as shown in Figure 3. This physical phenomenon results in significant color shifts observed in underwater images, making the images mainly shifted to blue and green. Therefore, the first task of underwater image enhancement is to correct the color shift of the image to restore its relatively real colors. Currently, color constancy-based methods have demonstrated their effectiveness for underwater image color correction. However, the color correction methods based on color constancy have certain limitations, they can correct the color deviation of the image for underwater images well with slight loss of red channel information, for serious loss of red channel information, the corrected underwater image produces significant red artifacts, as shown in Figure 6(d). These artifacts are caused by overcompensation in areas where red color appears, whereas red enhancement should primarily affect pixels with small red channel values and should not alter pixels that already contain significant red components [19]. In view of this, the present study explores a series of judgment methods aimed at accurately determining when the color constancy methods can be directly applied for correction and when additional processing of the red channel is required to avoid red artifacts during color correction.

After comprehensive consideration, we finally chose channel structure similarity [8] as our judgment criterion. The selection of channel similarity has several key advantages: first, it provides a comprehensive understanding of inter-channel relationships by comprehensively evaluating luminance, contrast, and structural information; second, this method demonstrates a high degree of accuracy and consistency in determining the relative informational richness between channels; Lastly, it effectively guides our compensation strategy to ensure that the intensity of the red channel is boosted while avoiding over-saturation and preserving the natural appearance of the image. Overall, channel similarity can be better used to measure the degree of information retention in the R, G, and B channels. Mathematically, the process of calculating channel similarity is as follows:

$$\mathrm{SSIM}(x, y) = \frac{\left(2\mu_x\mu_y + C_1\right)\left(2\sigma_{xy} + C_2\right)}{\left(\mu_x^2 + \mu_y^2 + C_1\right)\left(\sigma_x^2 + \sigma_y^2 + C_2\right)} \quad (1)$$

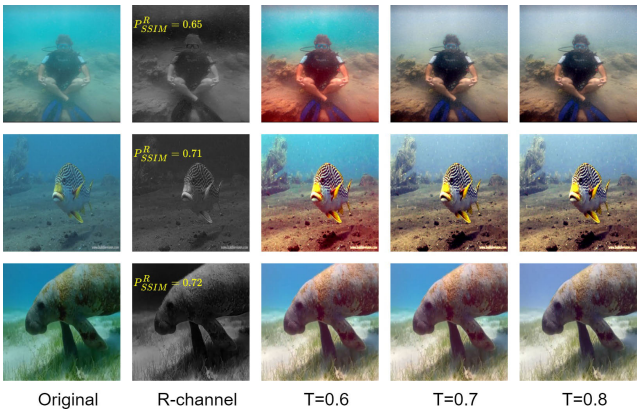

FIGURE 4. Comparison of color correction results at different T. Shows that the judgment condition with T set to 0.7 can obtain images with better contrast and color saturation.

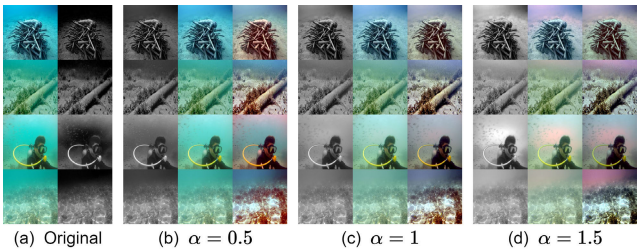

FIGURE 5. Visual comparison of red channel compensation effects. Image set (a) shows the original images and their red channels. Image sets (b), (c), and (d) each display the compensation effects when the compensation factor value is set to 0.5, 1, and 1.5, respectively. In each set of images, the first column shows the compensated red channel images, the second column presents the corresponding RGB images, and the third column illustrates the compensated color correction results, demonstrating the effect of the compensation process on the red channel and its subsequent color correction in the images.

where x, y represent the two channel images to be compared, μ_X, μ_y are the mean luminance of x, y respectively. σ_x^2,σ_y^2 are the variance of x, y respectively, σ_{xy} is the covariance of x and y, and $C1$, $C2$ are the stabilization factors.

We adopt the strategy of selecting the channel with the highest average pixel value and compute its similarity to the red channel. This strategy is based on the assumption that the color channel with the higher average pixel value commonly contains richer image information, which can provide a more accurate basis for evaluation. Thus, by comparing the structural similarity of these two channels, we are able to more effectively determine the degree of information loss in the red channel and adjust accordingly. In addition, since the green and blue channels show higher stability and consistency compared to the red channel in underwater environments, this study only directly calculates the structural similarity between these two channels in order to effectively evaluate their information retention status, and plays a key role in the color correction methods discussed subsequently in this paper. Specifically, our mathematical calculation equations are as follows:

$$P^{\mathrm{R}}_{\mathrm{SSIM}} = \begin{cases} \mathrm{SSIM}(I^{\mathrm{R}}, I^{\mathrm{G}}), & \text{if } P^{\mathrm{G}}_{\mathrm{mean}} > P^{\mathrm{B}}_{\mathrm{mean}} \\ \mathrm{SSIM}(I^{\mathrm{R}}, I^{\mathrm{B}}), & \text{if } P^{\mathrm{G}}_{\mathrm{mean}} < P^{\mathrm{B}}_{\mathrm{mean}} \end{cases} \tag{2}$$

$$P^{\mathrm{G}}_{\mathrm{SSIM}} = P^{\mathrm{B}}_{\mathrm{SSIM}} = \mathrm{SSIM}(I^{\mathrm{G}}, I^{\mathrm{B}}) \tag{3}$$

where $P^{\mathrm{R}}_{\mathrm{SSIM}}$ represents the SSIM value of the red channel with channel with maximum pixel average, I^{R}, I^{G}, and I^{B} respectively represent the R, G, and B channels of the original underwater image I. $P^{\mathrm{G}}_{\mathrm{mean}}$ and $P^{\mathrm{B}}_{\mathrm{mean}}$ represent the pixel average of the green channel and the pixel average of the blue channel, respectively. $P^{\mathrm{G}}_{\mathrm{SSIM}}$ and $P^{\mathrm{B}}_{\mathrm{SSIM}}$ represent the SSIM values of the green channel and the blue channel.

In our method, we introduce a threshold T to determine the necessity of color compensation for the red channel. When the value of $I^{\mathrm{R}}_{\mathrm{SSIM}}$ is greater than T, we consider that the structural similarity between the red channel and the maximum channel is sufficiently high that direct color correction can obtain satisfactory results. On the contrary, we need to apply color compensation before color correction to avoid over-processing the regions with sufficient red components. To accurately adjust the degree of color compensation for the red channel, we set the threshold T in the range of 0.6 to 0.8. Through observation and analysis, we notice that when T is set to 0.6, as shown in the first row of Figure 4, the color correction produces red artifacts. This indicates that under the condition that $P^{\mathrm{R}}_{\mathrm{SSIM}}$ is larger than 0.6 and smaller than 0.7, the information in the red channel is still lacking, so it is necessary to compensate the red channel before color correction to avoid red artifacts. When T is set to 0.8, it may lead to overcompensation, which reduces the contrast and saturation of the image, and this result is especially obvious in the last column of Figure 4. Therefore, based on the results of a large number of experimental tests, we determine that the best results can be achieved by performing color correction under the judgment condition of T equal to 0.7, which not only effectively avoids the generation of red artifacts, but also maintains the contrast and saturation of the image.

The color compensation strategy reconstructs the red channel based on the relative stability of the green channel. Because the compensation process takes into account the hypothetical theory in the Gray World [29] that the average value of each color channel is the same before light attenuation, and accordingly the degree of red compensation is quantified by the difference between the average values of the green and red channels. Meanwhile, the amount of compensation is considered at the pixel level. This allows the compensation to be flexibly adjusted to the specifics of the image, giving more compensation to areas with less red channel information and less compensation to areas with richer red channel information, resulting in a more natural and balanced visual effect. Based on this, the degree of red compensation is quantified through the difference in the average values of the green and red channels. Red channel

FIGURE 6. Shows the results of different color correction methods applied to underwater images. The original images is shown in column (a). Columns (b) to (f) show the images after applying the following color correction techniques respectively: Gray World [29], UCM [17], the method proposed by Fu et al. [21], the underwater white balance technique of Ancuti et al. [19] and our proposed color correction method.

compensation is obtained by the following equation:

$$I^{\mathrm{RC}}(x) = I^{\mathrm{R}}(x) + \alpha(P^{\mathrm{G}}_{\mathrm{mean}} - P^{\mathrm{R}}_{\mathrm{mean}})(1 - I^{\mathrm{R}}(x))I^{\mathrm{G}}(x) \quad (4)$$

$$I^{\mathrm{RN}}(x) = \begin{cases} I^{\mathrm{RC}}(x), & \text{if } P^{\mathrm{R}}_{\mathrm{SSIM}} \leq T \\ I^{\mathrm{R}}(x), & \text{if } P^{\mathrm{R}}_{\mathrm{SSIM}} > T \end{cases} \quad (5)$$

where I^{RC} represents the compensated red channel, $I^{\mathrm{R}}(x)$ and $I^{\mathrm{G}}(x)$ represent each pixel value of the original red channel and green channel, respectively. α is the compensation factor, and we set its value to 1. As shown in Figure 5, we experimentally test different values of α. The results show that when $\alpha = 0.5$, the red channels are undercompensated, and the images show red artifacts after color correction. On the contrary, when $\alpha = 1.5$, the overcompensation causes the images to show unnatural color distortion in local areas, which affects the overall visual effect of the images. When the compensation factor is set $\alpha = 1$, the best compensation effect can be achieved in different underwater lighting scenarios, which not only avoids the problem of under- or over-compensation, but also achieves a more natural and balanced color correction, which significantly improves the visual quality of underwater images.

B. ADAPTIVE COLOR CORRECTION BASED ON STATISTICS AND CHANNEL SIMILARITY

Corrections methods based on color statistics have been widely adopted in underwater image processing, mainly due to their ability to simply and efficiently adjust the color distribution in images. However, the traditional statistical-based approach has a significant limitation: it relies on a fixed constant parameter λ to control the dynamic range of the image. This approach can be problematic, as it does not account for the varying color distributions found in different underwater images. To address this limitation, we proposed a new strategy to adapt to the different color features of underwater images.

We calculate the mean and variance for each color channel, two statistical parameters that provide information about the color distribution for each image. At the same time, we combine the similarity value of each channel with the parameter λ to design a new adaptive normalization range to better control the dynamic range of the image. This allows our color correction method to adaptively and dynamically adjust based on the color distribution and statistical properties of each image, rather than relying solely on the λ value. The specific calculation equation is as follows:

$$P^{c_1}_{\mathrm{max}} = P^{c_1}_{\mathrm{mean}} + (\lambda + (1 - P^{c}_{\mathrm{SSIM}}))P^{c_1}_{\mathrm{var}} \quad (6)$$

$$P^{c_1}_{\mathrm{min}} = P^{c_1}_{\mathrm{mean}} - (\lambda + (1 - P^{c}_{\mathrm{SSIM}}))P^{c_1}_{\mathrm{var}} \quad (7)$$

where $c_1 \in \{\mathrm{RN}, \mathrm{G}, \mathrm{B}\}$, RC represents the red channel after color compensation, $P^{c}_{\mathrm{SSIM}} \in \{P^{\mathrm{R}}_{\mathrm{SSIM}}, P^{\mathrm{G}}_{\mathrm{SSIM}}, P^{\mathrm{B}}_{\mathrm{SSIM}}\}$, $P^{c_1}_{\mathrm{mean}}$ and $P^{c_1}_{\mathrm{var}}$ are the mean and variance of each color channel of the underwater image, respectively. P^{c}_{max} and P^{c}_{min} are the maximum and minimum values used for normalization. λ is a parameter controlling the dynamic range of the image, we evaluate the effect of different λ on color correction. The results show that too small λ leads to image distortion. $\lambda = 1$ results in severe distortion of the images, with the

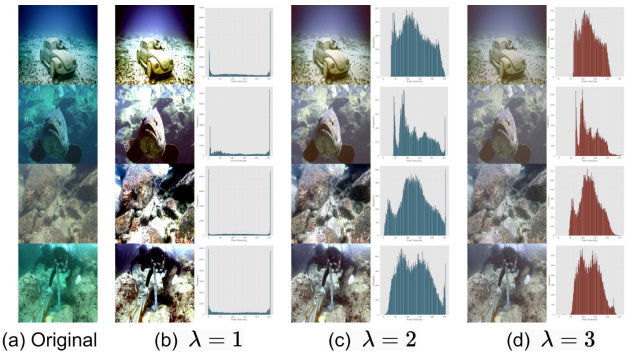

FIGURE 7. Visual comparison of color correction at different values of b. (a) are the original images. (b), (c) and (d) show the image processing results when b is set to 1, 2 and 3, respectively. In each set of images, the first column shows the color correction results and the second column is the histogram of the corresponding image processing results.

pixel distributions mainly concentrated at the two extremes. $\lambda = 3$ results in insufficient image contrast and blurred images. In contrast, $\lambda = 2$ provides the best color correction results, achieves a wide pixel distribution, and reasonably enhances the contrast, while preserving the details and clarity of the image, as shown in Figure 7(c). Then, we normalize I^{c_1} by mapping it to the range 0 to 255 using the following equation:

$$I^{c_1}_{\mathrm{COR}} = \frac{I^{c_1} - I^{c_1}_{\max}}{I^{c_1}_{\max} - I^{c_1}_{\min}} \times 255 \tag{8}$$

where $I^{c_1}_{\mathrm{COR}}$ represents the color corrected image.

As shown in Figure 6, our proposed color correction strategy can better balance the red channel, reduce the red artifacts introduced by domain stretching, and effectively correct the color shift of the underwater image, thus achieving a more realistic and saturated color effect. However, underwater images still have some inherent challenges that cannot be ignored. In particular, the image suffers from a lack of contrast due to the scattering and absorption effects of the water, thus making certain details disappear from view. Consequently, we will detail in the next section a frequency-domain based processing strategy for color-corrected underwater images. This strategy further optimizes the image quality by combining the stationary wavelet transform and sharpening techniques.

C. STATIONARY WAVELET TRANSFORM ENHANCES IMAGE DETAILS

Wavelet transform is widely applied in the image analysis and processing with its excellent properties demonstrated in key areas such as denoising [30], image enhancement [31], edge detection [32], and feature extraction [33]. The wavelet transform has been significantly developed and applied in the field of underwater image enhancement in recent years, especially in feature fusion [41], [49]. Underwater images face the challenge of blurring and distortion due to refraction and scattering of light in water, suspended particles, etc. Wavelet transform, due to its excellent ability

FIGURE 8. Comparison of results for images processed with different sharpening factors. (a) is the underwater image without detail enhancement after color correction. (b-d) are images after detail enhancement with sharpening factors of 0.2, 1 and 10, respectively.

in multi-scale analysis and preserving image details, has become an effective tool to deal with these challenges. In this work, we propose an enhancement method based on wavelet transform for single underwater image details, as shown in Figure 2. We aim to adopt a simple and efficient method that can make the objects and structures in underwater images more clearly recognizable, and further enhance the overall visibility and recognition of the images. We choose the simplest member of Daubechies wavelets, the db1 (Haar) wavelet. It is ideal for image detail enhancement in this study due to its simple form, computational efficiency, and ability to effectively capture edge and detail information in the image. Its scale function $\phi(x)$ and wavelet function $\varphi(x)$ can be defined as respectively:

$$\phi(x) = \begin{cases} 1 & \text{if } 0 \le x < 1 \\ 0 & \text{if } otherwise \end{cases} \tag{9}$$

$$\varphi(x) = \begin{cases} 1 & \text{if } 0 \le x < \frac{1}{2} \\ -1 & \text{if } \frac{1}{2} \le x < 1 \\ 0 & \text{if } othersize \end{cases} \tag{10}$$

Furthermore, $I^{c_1}_{\mathrm{COR}}(x, y)$ as the input image, its first level wavelet decomposition can be expressed as:

$$\mathrm{LL}^{c_1}(x, y) = I^{c_1}_{\mathrm{COR}}(x, y) * \phi(x) * \phi(y) \tag{11}$$

$$\mathrm{LH}^{c_1}(x, y) = I^{c_1}_{\mathrm{COR}}(x, y) * \phi(x) * \varphi(y) \tag{12}$$

$$\mathrm{HL}^{c_1}(x, y) = I^{c_1}_{\mathrm{COR}}(x, y) * \varphi(x) * \phi(y) \tag{13}$$

$$\mathrm{HH}^{c_1}(x, y) = I^{c_1}_{\mathrm{COR}}(x, y) * \varphi(x) * \varphi(y) \tag{14}$$

We use stationary wavelet transform (SWT) rather than discrete wavelet transform (DWT), because stationary wavelet has translation invariance and produces a stable response to small translations of the image. Meanwhile, SWT the image to the same size as the original image, this property of maintaining the original resolution allows for multi-scale analysis at the same spatial resolution, aiming to more accurately capture the details and structural features of the image. Additionally, stationary wavelet reserves all information in each decomposition, ensuring the completeness and continuity of the entire process.

The presence of particles and impurities in the water scatters the incident light, resulting in underwater images that show blurred object edges and lost details. Such problems are commonly concentrated in the low-frequency portion of

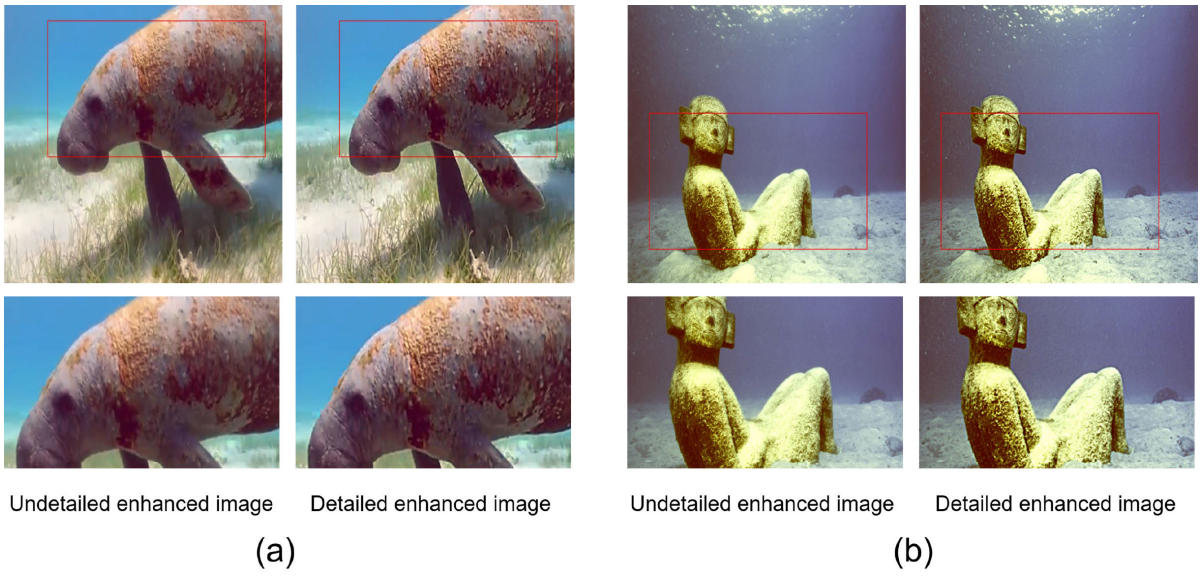

FIGURE 9. Comparison of the undetailed enhanced image and the detail enhanced image. The second row shows a magnified view of the selected area from the first row.

the image, which is the region of the image that contains the main structural and luminance information. To reduce the impact of underwater environmental factors on image quality, especially in low light and poor water quality conditions, we utilize Gaussian filters to process the low-frequency components of each channel of the image to obtain a blurred image. The specific process is as follows:

$$I_M^{c_1} = \mathrm{LL}^{c_1} * G_1 \, c_1 \in \{\mathrm{RN}, \mathrm{G}, \mathrm{B}\} \tag{15}$$

where $*$ represents the convolution operation, $I_M^{c_1}$ is the resulting blurred image, LL^{c_1} is the low-frequency component of each channel after color correction and G_1 is the Gaussian filter. With this step, we obtained a blurred image that emphasizes the main structures and objects of the image while removing the high-frequency noise and detail information. Subsequently, we calculate the difference image $I_F^{c_1}$ between LL^{c_1} and the blurred image $I_M^{c_1}$ by equation (16), finally the difference image is weighted and added back to the image LL^{c_1} according to equation (17) to get the detail enhanced image $\mathrm{LL}_E^{c_1}$.

$$I_F^{c_1} = \mathrm{LL}^{c_1} - I_M^{c_1} \tag{16}$$

$$\mathrm{LL}_E^{c_1} = \mathrm{LL}^{c_1} + \beta I_F^{c_1} \tag{17}$$

where β is an adjustable parameter that determines the degree of image sharpening. To determine the optimal value of β, we conducted many experiments to vary the size of the over-parameter β. The results of the sharpened image are found to be the best when the parameter $\beta = 1$, which can effectively enhance the contrast of the image and significantly improve the overall visual effect of the image, as shown in Figure 8(c). In contrast, when $\beta = 0.2$, the image detail enhancement is not significant and high-frequency details are not enhanced, resulting in the image remaining in a blurred state. When $\beta = 10$, the high-frequency details in the image are over-enhanced, especially at the image edges and texture regions, which leads to distortion of the image details and noise amplification, thus degrading the quality of the image. We only show the results of our single experiment in Figure 8, but we experimented with many sizes of the parameter β in fact.

For the high-frequency components, which are the details and textures in the image, we choose to leave them as they are without further processing. We consider that processing the detail information of the image too much will lead to loss of detail or noise amplification, and instead degrade the quality of the image. Therefore, we merge the detail-enhanced low-frequency subbands with the unprocessed high-frequency subbands and obtain the final reconstructed image by inverse wavelet transform. The specific calculation equation is as follows:

$$\begin{aligned} I_D^{c_1}(x,y) = {} & (\mathrm{LL}_E^{c_1}(x,y) * \phi^{-1}(x) * \phi^{-1}(y)) \\ & + (\mathrm{LH}^{c_1}(x,y) * \phi^{-1}(x) * \varphi^{-1}(y)) \\ & + (\mathrm{HL}^{c_1}(x,y) * \varphi^{-1}(x) * \phi^{-1}(y)) \\ & + (\mathrm{HH}^{c_1}(x,y) * \varphi^{-1}(x) * \varphi^{-1}(y)) \end{aligned} \tag{18}$$

where $I_D^{c_1}$ represents the channel obtained by inverse wavelet transform, $\phi^{-1}(x)$ and $\varphi^{-1}(x)$ are the inverse scale function and inverse wavelet function of Haar wavelet respectively. As shown in Figure 9, after our image detail enhancement process, the clarity of the image is significantly improved. Besides, the method also effectively enhances the details and contrast of the image and optimizes the overall visual effect of the image.

Since natural light is not available in deep-sea environments, relying on artificial light source illumination will result in the image showing uneven luminance distribution.

Algorithm 1 Outline of Proposed Algorithm

Input: I
Output: I_D

Decompose the input image I into R, G, B channels
$P^{\mathrm{R}}_{\mathrm{mean}}, P^{\mathrm{G}}_{\mathrm{mean}}, P^{\mathrm{B}}_{\mathrm{mean}} \leftarrow \mathrm{mean}(I^{\mathrm{R}}), \mathrm{mean}(I^{\mathrm{G}}), \mathrm{mean}(I^{\mathrm{B}})$
$P^{\mathrm{R}}_{\mathrm{SSIM}}, P^{\mathrm{G}}_{\mathrm{SSIM}}, P^{\mathrm{B}}_{\mathrm{SSIM}}$ are calculated by Eqs. (1)-(3)
if $P^{\mathrm{R}}_{\mathrm{SSIM}} \leq T$ **then**
    $I^{\mathrm{RN}} \leftarrow$ compensation of the I^{R} by Eq. (4)
else
    $I^{\mathrm{RN}} \leftarrow I^{\mathrm{R}}$
end if
for each $c_1 \in \{\mathrm{RN}, \mathrm{G}, \mathrm{B}\}$ **do**
    Calculate $P^{c_1}_{\mathrm{mean}}$ and $P^{c_1}_{\mathrm{var}}$
    Calculate $P^{c_1}_{\mathrm{max}}$ and $P^{c_1}_{\mathrm{min}}$ by Eqs. (6)(7)
    Color corrected image I^{c}_{COR} obtained by Eq. (8)
    $\mathrm{LL}^{c_1}, \mathrm{LH}^{c_1}, \mathrm{HL}^{c_1}, \mathrm{HH}^{c_1}$ are obtained using stationary wavelet transform by Eqs. (9)-(14)
    Apply Gaussian blur to the LL^{c_1} by Eq. (15)
    The differential image $I^{c_1}_F$ is obtained by Eq. (16)
    The detail enhanced image $\mathrm{LL}^{c_1}_E$ is obtained by Eq. (17)
    The enhanced image $I^{c_1}_D$ is obtained by performing the inverse wavelet transform
end for
Recombine the $I^{\mathrm{RN}}_D, I^{\mathrm{G}}_D, I^{\mathrm{B}}_D$ into the composite image I_D
$I_D \leftarrow \mathrm{CLAHE}(I_D)$
Return I_D

Therefore, we introduce CLAHE [34] at the end to equalize the histogram of local regions of the image, which further enhances the contrast of the underwater image and makes the detailed features of the image more prominent, while avoiding the problem of over-enhancement of the image that may be caused by the global histogram equalization. We give the algorithmic flow of the proposed method as shown in Algorithm 1.

IV. RESULTS AND DISCUSSION

In this section, we first introduce the experimental settings, including the dataset, the comparison methods, and the evaluation metrics. Next, we compare our method qualitatively and quantitatively with other representative methods to evaluate the performance of our proposed method. We also analyze the contribution of applying SWT in underwater image detail enhancement in this section, as well as the effect of applying CLAHE for luminance equalization in the final stage of the processing flow. In addition, we compare the runtime of the different methods to show their performance in terms of efficiency.

A. EXPERIMENT SETTINGS

1) DATASETS

In this paper, we conducted experiments based on the UIEB dataset [35], which contains 950 actual underwater images including various underwater scenes such as deep-sea fish, coral reefs, submarine cables, and so on. Our test set consisted of reference datasets and non-reference datasets. For the reference dataset, we selected 90 pairs of underwater images with reference images from UIEB and named it UIEBT90. It is worth pointing out in particular that these 90 pairs of images are not randomly selected, but are specifically chosen by the Ucolor method from the UIEB dataset for testing [42]. Using images that are not part of the training set as the test set can validate the performance of the deep learning method more effectively, ensuring the rigor of the experiments and the accuracy of the results. For the no-reference datasets, we considered the unpaired subset validation set of EUVP [36], the URPC2018 [37], and the UIQS dataset [38], containing 329, 800, and 3630 images, respectively. These datasets provide a challenging and diverse test environment as they cover many different types of underwater scenes and visual degradation phenomena. This allows us to conduct more comprehensive comparative experiments to verify the generalization ability of different methods under different underwater conditions and scenarios.

2) COMPARED METHODS

We compared our proposed method with eight state-of-the-art underwater enhancement techniques, including four conventional methods (UDCP [39], GDCP [40], MLLE [20], WWPF [41]) and four deep learning-based methods (Ucolor [42], U-shape [26], TOPAL [25], Semi-UIR [27]). We used the source code provided by the authors and their recommended parameter settings to achieve the best results.

3) EVALUATION METRICS

We used two types of image quality evaluation metrics to prove the effectiveness of our method. These include non-reference image quality evaluation metrics and full-reference image quality evaluation metrics. For non-reference image quality evaluation metrics, we selected UCIQE [43] and UIQM [44]. UCIQE evaluates the underwater image quality by the linear combination of color intensity, saturation and contrast, with larger values indicating better image quality. UIQM is another non-reference underwater image quality evaluation metric, which combines the brightness, contrast, and saturation of images, with larger values also indicating better image quality. For full-reference image quality evaluation metrics, we utilized PCQI [45]. PCQI evaluates the processing effect by comparing the contrast between the original image and the processed image in a localized area, with larger values indicating a better processing effect. The UCIQE, UIQM, and PCQI image quality evaluation metrics are widely used in the field of underwater image enhancement and are recognized as important criteria for assessing underwater image quality. They not only cover the scope of non-reference and full-reference image quality assessment, but also have been adopted

TABLE 1. The mean UIQM scores of different methods on UIEBT90, EUVP-Test, UPRC2018 and UIQS.The highest value in each row is represented by a bold number.

	Original	CLAHE (1994)	UDCP (2013)	GDCP (2018)	Ucolor (2021)	MLLE (2022)	TOPAL (2022)	U-shape (2023)	WWPF (2023)	Semi-UIR (2023)	Ours
UIEBT90	2.4745	2.7409	2.0180	2.0995	3.0305	1.9561	2.8994	3.0141	2.3900	2.9503	**3.0529**
EUVP-Test	2.3394	2.6219	2.1027	2.1755	2.9762	2.2875	2.7860	2.9258	2.5158	2.9150	**3.0676**
UPRC2018	2.3077	2.5398	2.0970	2.2433	2.9184	2.6036	2.7764	2.8993	2.7280	2.8173	**3.0548**
UIQS	2.4641	2.6795	2.1315	2.4002	2.9963	2.4112	2.8644	2.9705	2.6591	2.9582	**3.0261**

TABLE 2. The mean UCIQE scores of different methods on UIEBT90, EUVP-Test, UPRC2018 and UIQS.The highest value in each row is represented by a bold number.

	Original	CLAHE (1994)	UDCP (2013)	GDCP (2018)	Ucolor (2021)	MLLE (2022)	TOPAL (2022)	U-shape (2023)	WWPF (2023)	Semi-UIR (2023)	Ours
UIEBT90	0.5031	0.5527	0.5860	0.6141	0.5709	0.6216	0.5726	0.5748	**0.6241**	0.6188	0.6203
EUVP-Test	0.4742	0.5206	0.5996	0.5982	0.5628	0.6123	0.5403	0.5466	0.6155	0.5932	**0.6187**
UPRC2018	0.3902	0.4378	0.4941	0.5410	0.5119	0.5693	0.4710	0.5284	0.5782	0.5532	**0.5883**
UIQS	0.4321	0.4761	0.5128	0.5467	0.5317	0.5829	0.5004	0.5456	**0.5958**	0.5667	0.5804

TABLE 3. The mean PCQI scores of different methods on UIEBT90, EUVP-Test, UPRC2018 and UIQS.The highest value in each row is represented by a bold number.

	Original	CLAHE (1994)	UDCP (2013)	GDCP (2018)	Ucolor (2021)	MLLE (2022)	TOPAL (2022)	U-shape (2023)	WWPF (2023)	Semi-UIR (2023)	Ours
UIEBT90	—	1.2036	0.9324	1.0161	1.1033	1.2242	1.1377	1.0866	1.2187	1.1704	**1.2614**
EUVP-Test	—	1.1696	1.2711	1.1936	1.0271	1.3888	1.1109	0.9495	1.3333	1.2886	**1.4001**
UPRC2018	—	1.1947	1.2160	1.3119	1.2758	1.2506	1.1205	1.1004	1.2997	1.3247	**1.4359**
UIQS	—	1.2268	1.1041	1.2127	1.2121	1.3304	1.0899	1.2035	1.3002	1.2911	**1.3707**

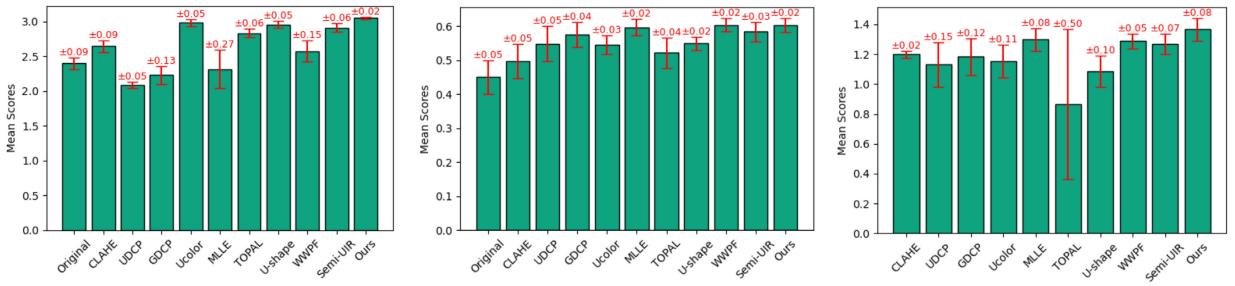

(a) UIQM Scores for Each Method with Standard Deviation

(b) UCIQE Scores for Each Method with Standard Deviation

(c) PCQI Scores for Each Method with Standard Deviation

FIGURE 10. Comparative analysis of mean scores and standard deviations of UIQM, UCIQE, and PCQI for each method on the dataset (UIEBT90, EUVP-Test, UPRC2018, UIQS). The error bars above each bar in the figure indicate the respective standard deviation.

by several state-of-the-art underwater image enhancement methods [19], [20], [26], [27], [41], [42], proving the wide recognition and reliability of their evaluation effects.

B. QUANTITATIVE COMPARISONS

We compared the quantitative results of our different methods on the UIEBT90, EUVP-Test, UPRC2018, and UIQS datasets, as shown in Table 1, 2, and 3. On the no-reference metrics, our method obtains the highest UIQM [44] scores on all four datasets, which reveals that our method performs better in enhancing the color and contrast of underwater images. As can be seen from the UCIQE [43] scores in Table 2, our method obtains the highest scores on both the EUVP-Test and UPRC2018 datasets, as well as the second-highest scores on the UIEBT90 and UIQS datasets, which indicates that our method is equally effective in color correction and clarity enhancement. As shown by the data in Table 3, our method also significantly outperforms the comparative methods in terms of the full reference metrics, as our method obtains the highest PCQI [45] scores on all four datasets, which demonstrates the significant improvement in perceptual quality achieved by our method as well, enhancing the realism and visual appeal of the images.

In addition, we conducted a comprehensive analysis of the UIQM, UCIQE, and PCQI scores obtained for each method on four datasets. Specifically, for each metric, we aggregated the scores obtained from the four datasets and then calculated the mean and standard deviation of these scores, which

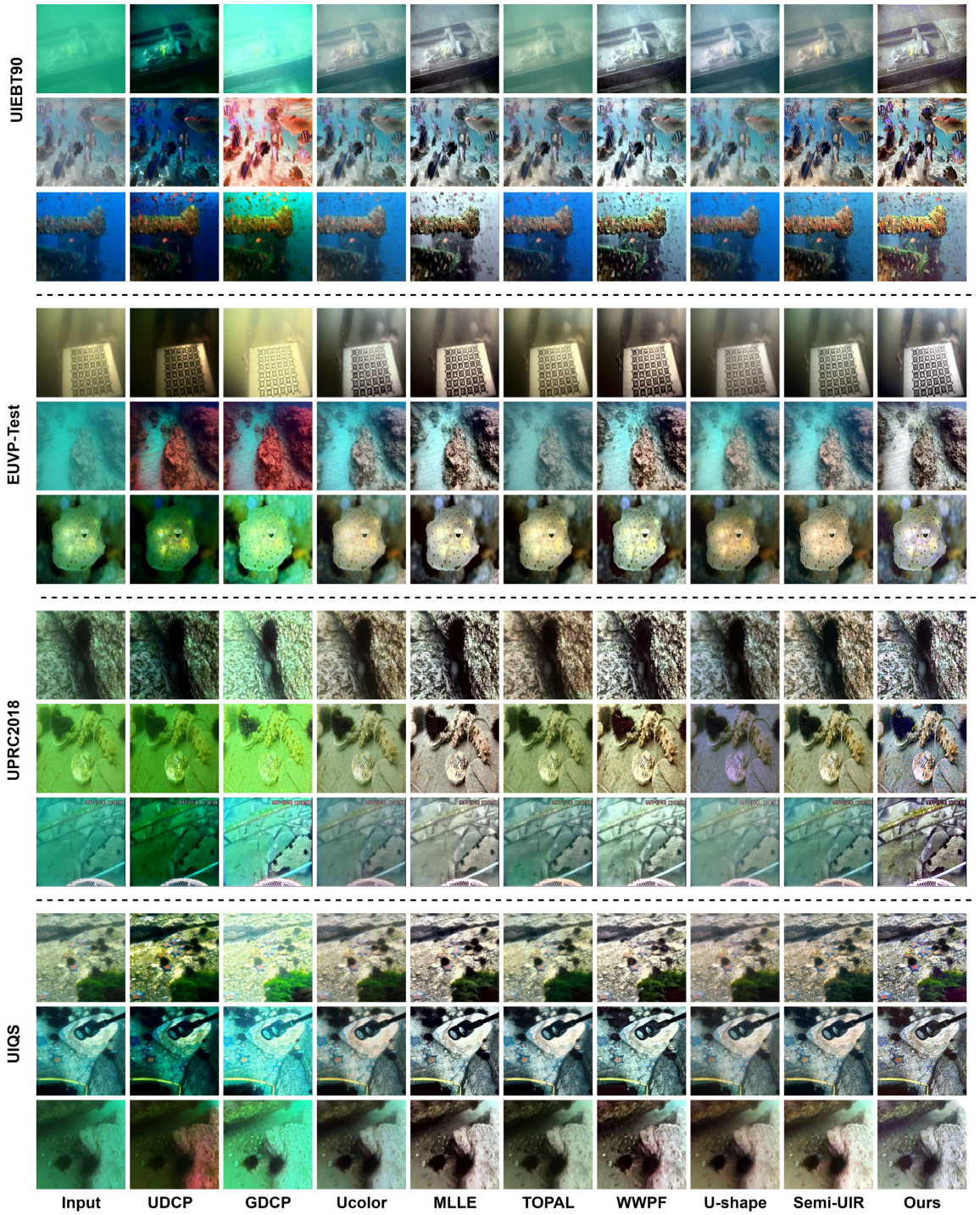

FIGURE 11. Visual comparison results of different methods.

allowed us to comprehensively evaluate the stability of each method in dealing with a variety of underwater environments. As shown in Figure 10, our method not only significantly outperforms several other traditional methods in mean UIQM scores, but also slightly outperforms deep learning-based Ucolor, U-shape, and Semi-UIR methods. Meanwhile, our method shows the smallest standard deviation, which indicates that our method can correct the color distortion of underwater images more consistently in different underwater environments. On the UCIQE and PCQI metrics, our method also shows high mean scores and small standard deviations. In contrast, the other methods have more fluctuating scores on these metrics and exhibit higher standard deviations, indicating that their performance is unstable on different

TABLE 4. The mean MSE, PSNR, and SSIM scores for image detail enhancement with and without SWT on the four datasets. ↓ indicates that the smaller the value, the better the image quality, ↑ indicates that the larger the value, the better.

	UIEBT90	EUVP-Test	UPRC2018	UIQS
MSE (Without SWT)	39.2644	38.0727	27.5943	32.1440
MSE (SWT Applied)	28.1458 ↓	25.1195 ↓	19.3769 ↓	22.5755 ↓
SSIM (Without SWT)	0.9084	0.9146	0.9136	0.9067
SSIM (SWT Applied)	0.9511 ↑	0.9521 ↑	0.9546 ↑	0.9516 ↑
PSNR (Without SWT)	26.8076	28.1237	30.7721	29.7518
PSNR (SWT Applied)	29.7342 ↑	30.6874 ↑	32.9939 ↑	32.0499 ↑

datasets. In the case of TOPAL, its scores on UCIQE and PCQI fluctuate significantly, reflecting a large difference in its performance on different datasets. This discrepancy may stem from the fact that TOPAL fails to fully learn certain dataset-specific underwater features during training. Overall, our method demonstrates significant advantages in all evaluation metrics, and these results not only highlight the excellent performance of our method but also prove its high stability in different underwater environments.

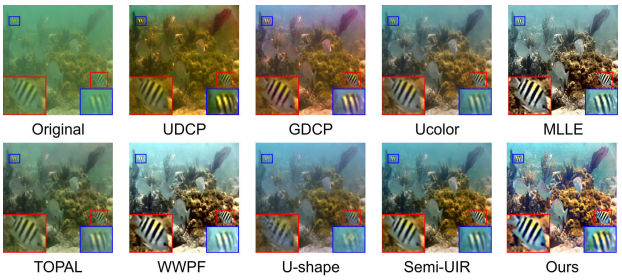

FIGURE 12. Comparison of different methods for texture detail enhancement in underwater images.

C. QUALITATIVE COMPARISONS

To demonstrate the superiority of our method, we qualitatively compared our results with other results of several state-of-the-art methods on four datasets. On each dataset, we selected underwater images of different underwater scenes to improve image visibility at different degradation levels, as shown in Figure 11. We first compared our method with traditional underwater image processing methods, including UDCP [39], GDCP [40], MLLE [20], and WWPF [41]. We found that UDCP significantly degrades image luminance and exacerbates color distortion, and even produces red artifacts when processing underwater images with green or blue deviation. GDCP enhances the overall luminance of the image but exacerbates the color distortion and tends to introduce red artifacts when processing light blue underwater scenes in the UIEBT90 and EUVB-Test datasets. MLLE and WWPF are able to achieve good results in underwater images, but they are not satisfactory in background color correction, and MLLE [20] and WWPF [41] also show slight red artifacts when processing blue-green underwater images in the UIQS dataset, as shown in the last row of images in Figure 11. These results indicate that although traditional methods can improve image quality in some aspects, they have limitations in color correction and avoiding artifacts.

In qualitative comparisons with deep learning-based underwater image enhancement methods, we analyze the performance of Ucolor [42], TOPAL [25], U-shape [26], and Semi-UIR [27] when processing images of different underwater scenes. Although these deep learning methods perform effectively in removing the effect of light scattering, they still face challenges in removing the background color deviation, as shown in the second row of images for the EUVP-Test dataset and the third row of images for the EUIB90 dataset in Figure 11. This problem may be mainly attributed to the fact that deep learning-based methods rely on a large amount of accurately labeled training data to learn and recognize complex underwater environment features. However, due to the diversity and complexity of underwater environments and the limitations of photographing under real conditions, it is difficult to obtain a sufficiently large and realistic number of labeled images. This leads to the result that deep learning models may not be able to adequately learn and adapt to variable underwater environments during training.

In comparison, Our method not only obtained excellent color correction results when processing underwater images with blue and green deviations, but also better eliminated the color deviation of the background. Moreover, our method can better improve the clarity of yellow turbid underwater images. Overall, our method obtained excellent color correction results in any color-shifted underwater scene, outperforming comparative methods in terms of color correction, contrast enhancement, brightness enhancement, and detailed texture enhancement. This reflects the excellent performance of our method in color correction and detail enhancement, which also proves that in the field of underwater image enhancement, traditional methods still have their unique and irreplaceable advantages in some aspects, especially in dealing with image background color deviation.

D. EVALUATION OF DETAIL ENHANCEMENT APPLYING STATIONARY WAVELET TRANSFORM

To comprehensively evaluate our proposed image detail enhancement strategy based on SWT, we designed a set of comparison experiments. Specifically, in the strategy with SWT, we first performed wavelet decomposition on the

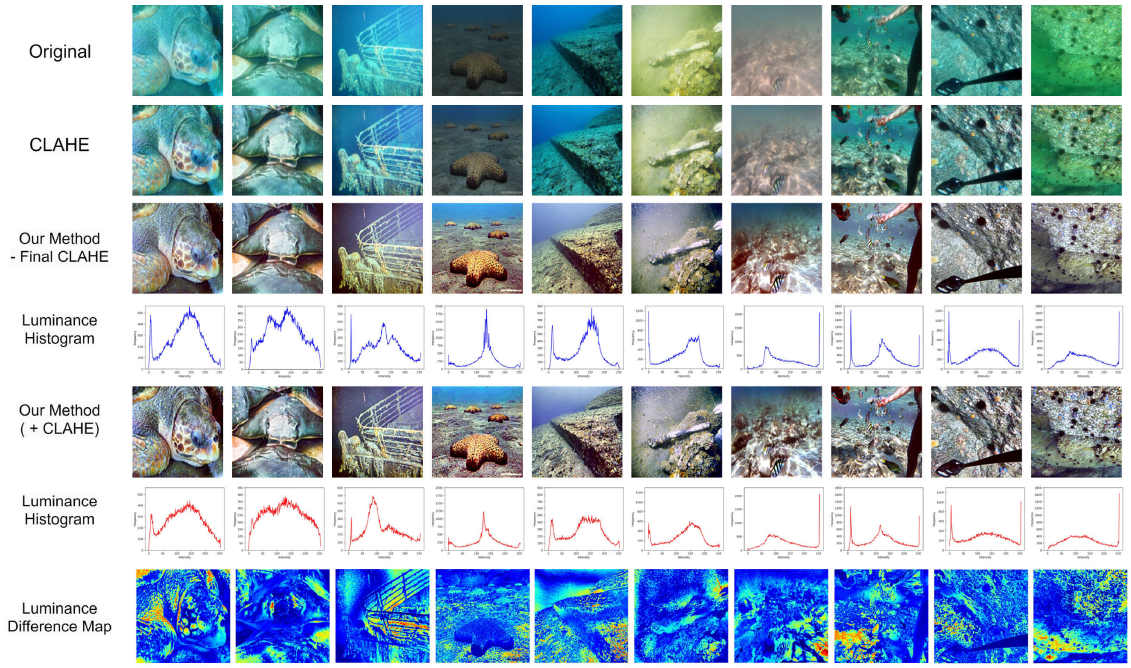

FIGURE 13. Visual comparison of the impact of CLAHE on our underwater image enhancement method performance. The first row shows the original image; the second row shows the image processed only using CLAHE; the third and fifth rows show the results of our method without applying and after applying the final CLAHE step, respectively; the fourth and sixth rows provide luminance histograms corresponding to the images in the third and fifth rows, respectively, which are used to quantitatively analyze the luminance distributions; and the last row shows a graph of the luminance difference between the third and fifth rows of the image, which visually compares the luminance changes.

input image and then performed detail enhancement on the obtained low-frequency components and reconstructed them by inverse wavelet transform to obtain the detail-enhanced image. While in the strategy without SWT, we directly performed the same detail enhancement process on the input image to obtain the enhanced image. The purpose of this set of comparison experiments is to clearly demonstrate the effect of applying SWT in underwater image detail enhancement and its advantages. We evaluated their performance using quantitative metrics of MSE, PSNR [48], and SSIM.

As shown in Table 4, the PSNR and SSIM of the enhancement strategy using SWT are higher than those of the strategy without SWT on four datasets, and its MSE metric is also lower, demonstrating that the strategy based on SWT effectively enhances image details while avoiding the introduction of too much noise. In addition, we evaluated the performance of our method in enhancing texture details compared to several other state-of-the-art methods, as shown in Figure 12. By locally magnifying the area, it can be observed that MLLE [20], WWPF [41], and our method effectively enhanced the texture information in the red-boxed area, significantly improving its contrast and clarity. However, our method outperforms MLLE and WWPF in the blue-boxed annotation area, making the colors more saturated and significantly improving image clarity. This shows that our detail enhancement strategy based on SWT has significant advantages over other state-of-the-art methods in enhancing texture information, contrast, and saturation.

TABLE 5. The mean scores of UIQM, UCIQE, and PCQI for our method applying CLAHE and without CLAHE on the four datasets. The highest value in each row is represented by a bold number.

		Original	Ours (-Final CLAHE)	Ours
UIQM	UIEBT90	2.4745	2.7241	**3.0529**
	EUVP-Test	2.3394	2.7249	**3.0676**
	UIQS	2.4641	2.6914	**3.0261**
	UPRC2018	2.3077	2.7186	**3.0548**
UCIQE	UIEBT90	0.5031	0.6164	**0.6203**
	EUVP-Test	0.4742	**0.6188**	0.6187
	UIQS	0.4321	**0.5900**	0.5804
	UPRC2018	0.3902	0.5848	**0.5883**
PCQI	UIEBT90	—	1.1588	**1.2614**
	EUVP-Test	—	1.3646	**1.4001**
	UIQS	—	1.3112	**1.3707**
	UPRC2018	—	1.3435	**1.4359**

E. EVALUATION OF CLAHE ON UNDERWATER IMAGE ENHANCEMENT

This section introduces a comparative study aimed at comprehensively evaluating the specific impact of CLAHE on the performance of our underwater image enhancement method. We designed three sets of experiments: the first set of experiments only applied CLAHE to process underwater images; the second set of experiments applied our complete image enhancement process, which includes luminance equalization using CLAHE in the final step; and the third set

TABLE 6. The mean runtime of on 300 images of size 256 × 256 for each method. The fastest runtime value in row is represented by a bold number.

Method	UDCP	GDCP	Ucolor	MLLE	TOPAL	U-shape	WWPE	Semi-UIR	Ours
Time (s)	2.0196	0.1350	6.6448	**0.0557**	1.1002	0.5056	0.2260	0.6221	0.3767

of experiments applied our enhancement method but removed the CLAHE step in the process. Such experimental setup is intended to reveal the unique contribution of CLAHE in the whole enhancement process and its impact on the final image quality.

Through the comparison of the third and fifth rows of images in Figure 13, we can observe that the image quality has been significantly improved and the color distortion problem has been effectively solved after the steps of color correction and detail enhancement. Nevertheless, these images still need to be optimized in luminance distribution. By applying CLAHE in the last step, the image luminance has been significantly adjusted, resulting in a more uniform luminance distribution, as shown in the luminance histograms in the fourth and fifth rows of Figure 13. To visualize the impact of CLAHE even more, the last row of Figure 13 provides maps of the difference in luminance with and without CLAHE in the final step. These comparison images clearly reveal the effect of CLAHE as the last step of our method in terms of adjusting the luminance of the image.

To further evaluate the impact of CLAHE on the performance of our underwater image enhancement method, we conducted a series of quantitative comparisons. UIQM, UCIQE, and PCQI were selected as the quantitative evaluation metrics, and we focused on analyzing the effect of applying CLAHE on image quality enhancement at the final stage of the processing flow. Table 5 demonstrates the comparison of UIQM, UCIQE, and PCQI scores of our method with and without applying CLAHE on four different datasets. The data in Table 5 show that when CLAHE is used in the final stage of processing, our method outperforms the case without CLAHE in most metrics, and the improvement in UIQM scores is particularly significant. This result demonstrates that the luminance and contrast of the images are significantly improved by applying CLAHE. Although the UCIQE scores decreased after applying CLAHE, this demonstrates that the preliminary stage of our method has been effective in improving the color correction of the images, and that further enhancement of luminance may lead to subtle color variations that can affect the UCIQE scores. However, considering that our goal is to address the luminance distribution of underwater images and further enhance the image quality, subtle color variations are acceptable, especially considering the significant enhancement of the images in terms of luminance and contrast.

F. COMPARISONS OF RUNTIME

To evaluate the computational complexity of our method, we randomly selected 300 underwater images from four test datasets for runtime comparison. The experiments were run on a Windows 10 PC with Intel(R) Core(TM) i9−9900k CPU at 3.6 GHz, 32 GB Memory, Matlab2018b, and Python 3.8. As can be seen from the data in Table 6, our algorithm ranks fourth among all tested algorithms in terms of mean running time, which is slightly higher than MLLE, WWPF, and GDCP, but better than several deep learning-based methods (Ucolor, U-shape, TOPAL, and Semi-UIR). This result reveals the balance between the running efficiency and the processing quality of our algorithm, particularly in comparison to the deep-learning-based algorithms. This may be due to the fact that our algorithms are designed to run more efficiently in traditional CPU environments without relying on GPU acceleration, which is especially important in resource-constrained application environments. In the future, we plan to further optimize the running speed of our algorithm while trying to maintain or improve the quality of image processing.

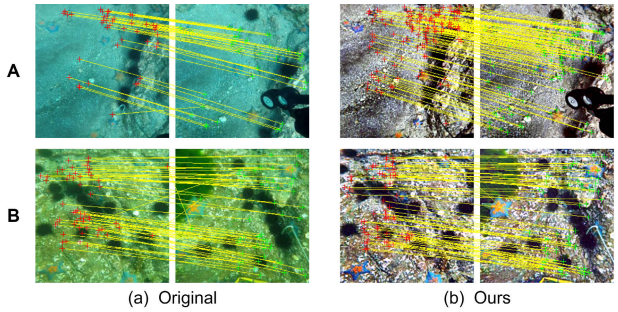

FIGURE 14. Shows the result of applying the SIFT operator to match key feature points on underwater images. where (a) is the key point matching effect of the original underwater images and (b) is the key point matching effect of the underwater images enhanced with our method. The quantitative evaluation based on SIFT matching is shown in Table 7.

TABLE 7. Statistics of the number of correct and incorrect matches for applying the SIFT operator to match key feature points on two sets of underwater images A and B in Figure 14. ↓ indicates that the smaller the value, the fewer the number of incorrect matches, and ↑ indicates that the larger the value, the more correct matches.

Underwater pair of images	Correct Matches	Incorrect Matches
A Original	45	1
A Ours	126 ↑	1
B Original	54	3
B Ours	73 ↑	1 ↓

V. APPLICATION

Image processing aims to optimize image quality and provide high-quality images for further analysis and applications. Therefore, to verify the performance of underwater images

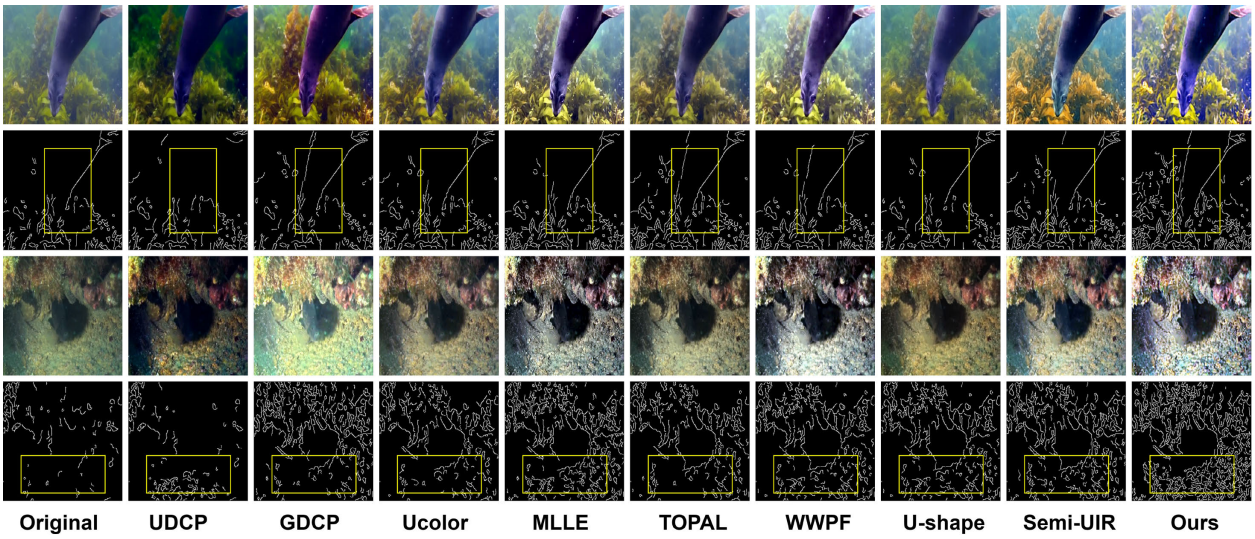

FIGURE 15. Example application of edge detection for underwater images applying Canny operator.

processed by our method for practical applications, we will analyze its performance on two major applications of key feature point matching and image edge detection.

A. UNDERWATER IMAGE KEY FEATURE MATCHING

We applied the standard SIFT operator [46] to compute keypoint matching on both the original and the processed underwater images of our method, such as the two sets of underwater images A and B shown in Figure 14. It can be clearly seen that the underwater images processed by our method are able to detect and match more feature points, both in group A images and group B images. The data in Table 7 shows that for the original underwater images in group A1, 45 correct keypoint matches and 1 wrong match were found by applying the SIFT operator. When the SIFT operator is applied to the images processed by our method, the number of correct keypoint matches on group A images increases to 126 with only 1 incorrect match, and the number of correct keypoint matches on group B images increases to 73, with only 1 incorrect match. Quantitative and qualitative results show that our method of underwater image enhancement not only improves the number of feature point matching, but also enhances the accuracy of matching. It effectively improves the image quality and makes the key information in the image clearer and more accurate.

B. EVALUATION OF DETAIL ENHANCEMENT

Edge detection has become one of the notable applications as it not only reveals the key structural and shape information of the image but also helps to enhance the clarity of the target and improve the recognizability of the image. As shown in Figure 15, we applied the Canny operator [47] for edge detection and compared the original image as well as the image enhanced by different methods. In Figure 15, the first and third rows are the original images and the images processed by each method, and the second and fourth rows are the Canny edge detection results corresponding to each image in the first and third rows respectively. As can be seen in the second row of images, the underwater images enhanced by our methods have more complete edges, the contour edges of marine organisms are more complete, and the edges of seagrasses are richer. In the fourth row of comparison, the underwater image enhanced by our method has more edge information while the background contours in the image are clearer. This proves the excellent performance of our method for edge detection applications.

VI. CONCLUSION

In this paper, we introduce in detail a novel method for underwater image enhancement. The method cleverly combines statistical color correction and stationary wavelet detail enhancement techniques. By introducing the channel similarity value as a judgment criterion for color compensation and combining it with statistical color correction methods, our method is not only applicable to the processing of various underwater scenes, but also more accurately restores the real underwater colors. Additionally, the application of stationary wavelet decomposition further enhances the image details. Through extensive experimental evaluations, our method demonstrates superiority both qualitatively and quantitatively. In comparison with several other state-of-the-art methods, our proposed method exhibits superior performance in improving underwater image quality while demonstrating higher robustness. Meanwhile, application experiments show that our method also achieves excellent performance in practical applications such as keypoint matching and edge detection.

REFERENCES

[1] A. Saleh, M. Sheaves, and M. R. Azghadi, "Computer vision and deep learning for fish classification in underwater habitats: A survey," *Fish Fisheries*, vol. 23, no. 4, pp. 977–999, Apr. 2022.

[2] I. Dumke, M. Ludvigsen, S. L. Ellefmo, F. Søreide, G. Johnsen, and B. J. Murton, "Underwater hyperspectral imaging using a stationary platform in the trans-atlantic geotraverse hydrothermal field," *IEEE Trans. Geosci. Remote Sens.*, vol. 57, no. 5, pp. 2947–2962, May 2019.

[3] K. Gormley, F. McLellan, C. McCabe, C. Hinton, J. Ferris, D. Kline, and B. Scott, "Automated image analysis of offshore infrastructure marine biofouling," *J. Mar. Sci. Eng.*, vol. 6, no. 1, p. 2, Jan. 2018.

[4] F. Bruno, G. Bianco, M. Muzzupappa, S. Barone, and A. V. Razionale, "Experimentation of structured light and stereo vision for underwater 3D reconstruction," *ISPRS J. Photogramm. Remote Sens.*, vol. 66, no. 4, pp. 508–518, Jul. 2011.

[5] P. Zieliński and U. Markowska-Kaczmar, "3D robotic navigation using a vision-based deep reinforcement learning model," *Appl. Soft Comput.*, vol. 110, Oct. 2021, Art. no. 107602.

[6] A. S. A. Ghani and N. A. M. Isa, "Underwater image quality enhancement through integrated color model with Rayleigh distribution," *Appl. Soft Comput.*, vol. 27, pp. 219–230, Feb. 2015.

[7] H. Lu, Y. Li, Y. Zhang, M. Chen, S. Serikawa, and H. Kim, "Underwater optical image processing: A comprehensive review," *Mobile Netw. Appl.*, vol. 22, no. 6, pp. 1204–1211, Apr. 2017.

[8] A. Horé and D. Ziou, "Image quality metrics: PSNR vs. SSIM," in *Proc. 20th Int. Conf. Pattern Recognit.*, Aug. 2010, pp. 2366–2369.

[9] P. V. Teixeira, D. Fourie, M. Kaess, and J. J. Leonard, "Dense, sonar-based reconstruction of underwater scenes," in *Proc. IEEE/RSJ Int. Conf. Intell. Robots Syst. (IROS)*, Nov. 2019, pp. 8060–8066.

[10] Y. Zhao, W. He, H. Ren, Y. Li, and Y. Fu, "Polarization descattering imaging through turbid water without prior knowledge," *Opt. Lasers Eng.*, vol. 148, Jan. 2022, Art. no. 106777.

[11] S. Raveendran, M. D. Patil, and G. K. Birajdar, "Underwater image enhancement: A comprehensive review, recent trends, challenges and applications," *Artif. Intell. Rev.*, vol. 54, no. 7, pp. 5413–5467, Jun. 2021.

[12] J. S. Jaffe, "Computer modeling and the design of optimal underwater imaging systems," *IEEE J. Ocean. Eng.*, vol. 15, no. 2, pp. 101–111, Apr. 1990.

[13] J. Y. Chiang and Y.-C. Chen, "Underwater image enhancement by wavelength compensation and dehazing," *IEEE Trans. Image Process.*, vol. 21, no. 4, pp. 1756–1769, Apr. 2012.

[14] K. He, J. Sun, and X. Tang, "Single image haze removal using dark channel prior," *IEEE Trans. Pattern Anal. Mach. Intell.*, vol. 33, no. 12, pp. 2341–2353, Dec. 2011.

[15] P. L. J. Drews, E. R. Nascimento, S. S. C. Botelho, and M. F. M. Campos, "Underwater depth estimation and image restoration based on single images," *IEEE Comput. Graph. Appl.*, vol. 36, no. 2, pp. 24–35, Mar. 2016.

[16] D. Akkaynak and T. Treibitz, "Sea-thru: A method for removing water from underwater images," in *Proc. IEEE/CVF Conf. Comput. Vis. Pattern Recognit. (CVPR)*, Jun. 2019, pp. 1682–1691.

[17] K. Iqbal, M. Odetayo, A. James, R. A. Salam, and A. Z. Hj Talib, "Enhancing the low quality images using unsupervised colour correction method," in *Proc. IEEE Int. Conf. Syst., Man Cybern.*, Oct. 2010, pp. 1703–1709.

[18] L. Dong, W. Zhang, and W. Xu, "Underwater image enhancement via integrated RGB and LAB color models," *Signal Process., Image Commun.*, vol. 104, May 2022, Art. no. 116684.

[19] C. O. Ancuti, C. Ancuti, C. De Vleeschouwer, and P. Bekaert, "Color balance and fusion for underwater image enhancement," *IEEE Trans. Image Process.*, vol. 27, no. 1, pp. 379–393, Jan. 2018.

[20] W. Zhang, P. Zhuang, H.-H. Sun, G. Li, S. Kwong, and C. Li, "Underwater image enhancement via minimal color loss and locally adaptive contrast enhancement," *IEEE Trans. Image Process.*, vol. 31, pp. 3997–4010, 2022.

[21] X. Fu, P. Zhuang, Y. Huang, Y. Liao, X.-P. Zhang, and X. Ding, "A retinex-based enhancing approach for single underwater image," in *Proc. IEEE Int. Conf. Image Process. (ICIP)*, Oct. 2014, pp. 4572–4576.

[22] P. Zhuang, C. Li, and J. Wu, "Bayesian retinex underwater image enhancement," *Eng. Appl. Artif. Intell.*, vol. 101, May 2021, Art. no. 104171.

[23] X. Fu and X. Cao, "Underwater image enhancement with global–local networks and compressed-histogram equalization," *Signal Process., Image Commun.*, vol. 86, Aug. 2020, Art. no. 115892.

[24] J. Li, K. A. Skinner, R. M. Eustice, and M. Johnson-Roberson, "WaterGAN: Unsupervised generative network to enable real-time color correction of monocular underwater images," *IEEE Robot. Autom. Lett.*, vol. 3, no. 1, pp. 387–394, Jan. 2018.

[25] Z. Jiang, Z. Li, S. Yang, X. Fan, and R. Liu, "Target oriented perceptual adversarial fusion network for underwater image enhancement," *IEEE Trans. Circuits Syst. Video Technol.*, vol. 32, no. 10, pp. 6584–6598, Oct. 2022.

[26] L. Peng, C. Zhu, and L. Bian, "U-shape transformer for underwater image enhancement," *IEEE Trans. Image Process.*, vol. 32, pp. 3066–3079, 2023.

[27] S. Huang, K. Wang, H. Liu, J. Chen, and Y. Li, "Contrastive semi-supervised learning for underwater image restoration via reliable bank," in *Proc. IEEE/CVF Conf. Comput. Vis. Pattern Recognit. (CVPR)*, Jun. 2023, pp. 18145–18155.

[28] W. Zhang, G. Li, and Z. Ying, "A new underwater image enhancing method via color correction and illumination adjustment," in *Proc. IEEE Vis. Commun. Image Process. (VCIP)*, Dec. 2017, pp. 1–4.

[29] G. Buchsbaum, "A spatial processor model for object colour perception," *J. Franklin Inst.*, vol. 310, no. 1, pp. 1–26, Jul. 1980.

[30] Q. Pan, L. Zhang, G. Dai, and H. Zhang, "Two denoising methods by wavelet transform," *IEEE Trans. Signal Process.*, vol. 47, no. 12, pp. 3401–3406, Dec. 1999.

[31] C.-T. Hsieh, E. Lai, and Y.-C. Wang, "An effective algorithm for fingerprint image enhancement based on wavelet transform," *Pattern Recognit.*, vol. 36, no. 2, pp. 303–312, Feb. 2003.

[32] N. You, L. Han, D. Zhu, and W. Song, "Research on image denoising in edge detection based on wavelet transform," *Appl. Sci.*, vol. 13, no. 3, p. 1837, Jan. 2023.

[33] D. A. Zebari, H. Haron, S. R. Zeebaree, and D. Q. Zeebaree, "Mixture contrast limited adaptive histogram equalization for underwater image enhancement," in *Proc. Int. Conf. Adv. Sci. Eng. (ICOASE)*, 2019, pp. 100–105.

[34] M. S. Hitam, E. A. Awalludin, W. N. J. Hj Wan Yussof, and Z. Bachok, "Mixture contrast limited adaptive histogram equalization for underwater image enhancement," in *Proc. Int. Conf. Comput. Appl. Technol. (ICCAT)*, Jan. 2013, pp. 1–5.

[35] C. Li, C. Guo, W. Ren, R. Cong, J. Hou, S. Kwong, and D. Tao, "An underwater image enhancement benchmark dataset and beyond," *IEEE Trans. Image Process.*, vol. 29, pp. 4376–4389, 2020.

[36] M. J. Islam, Y. Xia, and J. Sattar, "Fast underwater image enhancement for improved visual perception," *IEEE Robot. Autom. Lett.*, vol. 5, no. 2, pp. 3227–3234, Apr. 2020.

[37] L. Chen, Z. Liu, L. Tong, Z. Jiang, S. Wang, J. Dong, and H. Zhou, "Underwater object detection using invert multi-class AdaBoost with deep learning," in *Proc. Int. Joint Conf. Neural Netw. (IJCNN)*, Jul. 2020, pp. 1–8.

[38] R. Liu, X. Fan, M. Zhu, M. Hou, and Z. Luo, "Real-world underwater enhancement: Challenges, benchmarks, and solutions under natural light," *IEEE Trans. Circuits Syst. Video Technol.*, vol. 30, no. 12, pp. 4861–4875, Dec. 2020.

[39] P. Drews, Jr., E. do Nascimento, F. Moraes, S. Botelho, and M. Campos, "Transmission estimation in underwater single images," in *Proc. IEEE Int. Conf. Comput. Vis. Workshops*, Dec. 2013, pp. 825–830.

[40] Y.-T. Peng, K. Cao, and P. C. Cosman, "Generalization of the dark channel prior for single image restoration," *IEEE Trans. Image Process.*, vol. 27, no. 6, pp. 2856–2868, Jun. 2018.

[41] W. Zhang, L. Zhou, P. Zhuang, G. Li, X. Pan, W. Zhao, and C. Li, "Underwater image enhancement via weighted wavelet visual perception fusion," *IEEE Trans. Circuits Syst. Video Technol.*, early access, Jul. 27, 2023, doi: 10.1109/TCSVT.2023.3299314.

[42] C. Li, S. Anwar, J. Hou, R. Cong, C. Guo, and W. Ren, "Underwater image enhancement via medium transmission-guided multi-color space embedding," *IEEE Trans. Image Process.*, vol. 30, pp. 4985–5000, 2021.

[43] M. Yang and A. Sowmya, "An underwater color image quality evaluation metric," *IEEE Trans. Image Process.*, vol. 24, no. 12, pp. 6062–6071, Dec. 2015.

[44] K. Panetta, C. Gao, and S. Agaian, "Human-visual-system-Inspired underwater image quality measures," *IEEE J. Ocean. Eng.*, vol. 41, no. 3, pp. 541–551, Jul. 2016.

[45] S. Wang, K. Ma, H. Yeganeh, Z. Wang, and W. Lin, "A patch-structure representation method for quality assessment of contrast changed images," *IEEE Signal Process. Lett.*, vol. 22, no. 12, pp. 2387–2390, Dec. 2015.

[46] D. G. Lowe, "Distinctive image features from scale-invariant keypoints," *Int. J. Comput. Vis.*, vol. 60, no. 2, pp. 91–110, Nov. 2004.

[47] J. Canny, "A computational approach to edge detection," *IEEE Trans. Pattern Anal. Mach. Intell.*, vol. PAMI-8, no. 6, pp. 679–698, Nov. 1986.

[48] J. Korhonen and J. You, "Peak signal-to-noise ratio revisited: Is simple beautiful?" in *Proc. 4th Int. Workshop Quality Multimedia Exper.*, Jul. 2012, pp. 37–38.
[49] Y. Wang, X. Ding, R. Wang, J. Zhang, and X. Fu, "Fusion-based underwater image enhancement by wavelet decomposition," in *Proc. IEEE Int. Conf. Ind. Technol. (ICIT)*, Mar. 2017, pp. 1013–1018.

ZHENBO WANG is currently pursuing the bachelor's degree in intelligent science and technology with the Beijing Institute of Technology, Zhuhai. Since 2021, he has been a Laboratory Member with the Intelligent Vision Research and Innovation Center, Beijing Institute of Technology. His research interests include underwater image enhancement, computer vision, and artificial intelligence.

DUJUAN ZHOU received the B.S. and M.S. degrees from the Nanjing University of Information Science and Technology, Nanjing, China, in 2003 and 2006, respectively. She is currently a Lecturer with the Beijing Institute of Technology, Zhuhai, China. Her research interests include signal and image processing, applied statistics, and queuing theory.

ZHICHUANG LI is currently pursuing the bachelor's degree in information engineering with the Beijing Institute of Technology, Zhuhai. His research interests include the application of deep learning in fields, such as machine vision and communications, and image processing.

ZIZHAO YUAN is currently pursuing the bachelor's degree in intelligent science and technology with the Beijing Institute of Technology, Zhuhai. He is an active member of the Smart Vision Research and Innovation Center, Beijing Institute of Technology. His research interests include underwater image enhancement and operator learning.

CHUN YANG is currently pursuing the bachelor's degree in information engineering with the Beijing Institute of Technology, Zhuhai. She is interested in the fields of underwater image processing, machine learning, and computer vision. She has consistently demonstrated dedication to the studies and has successfully applied theoretical knowledge to real-world problems. She obtained a technological patent and authored a paper presented at an international conference. She is active in research and innovation. She has participated in a National Innovative and Entrepreneurial Training Program for college students. Collaborating with the team, she has developed technological solutions with promising applications. Her expertise and innovative approach have earned numerous accolades, including five national awards and four provincial honors, underscoring the achievements in the field of study. With an eye on the future, she is determined to pursue master's studies following graduation, with the goal of furthering the academic and research capabilities in information engineering.